Improving High-Speed Interconnect Modeling: The Theta-Method for Accurate Simulation of Skin Effect and Computational Efficiency

Mouaad Ait errais[1], *Khaoula* Ait Belaid[2,3], *Hassan* Belahrach[3], and *Abdelouhab* Zeroual[1]

[1]Instrumentation, Signals, and Physical Systems (I2SP), Cadi Ayyad University, Marrakesh, Morocco
[2]Wolfson School of Mechanical, Electrical, and Manufacturing Engineering, Loughborough University, Loughborough, UK
[3]Laboratory of Electrical Systems, Energy Efficiency, and Telecommunications (LSEEET), Cadi Ayyad University, Marrakesh, Morocco

Abstract. This paper presents a novel θ-method for modeling coupled interconnects in high-speed electronic circuits, addressing the limitations of conventional Finite-Difference Time-Domain (FDTD) techniques. The proposed method enhances simulation efficiency and accuracy, particularly in scenarios involving high frequencies and the skin effect. Through comparative analyses with established FDTD methods, we demonstrate that the θ-method not only achieves significantly shorter computation times but also provides greater accuracy and stability. The results indicate that the θ-method is a robust and reliable alternative, offering improved performance in both simulation speed and precision for complex interconnect modeling tasks.

1 Introduction

As the trend toward miniaturization in Very-Large-Scale Integration (VLSI) continues, integrating billions of transistors onto a single chip brings both significant benefits and notable challenges [1]. This dense integration results in smaller, more powerful devices with increased functionality. However, it also leads to highly complex circuits, with interconnects (tiny wires that link the transistors) becoming the primary source of delay and power dissipation [2], ultimately constraining the performance of the integrated circuit [3]. Despite their role in creating challenges, interconnects also offer remarkable versatility. Beyond their traditional function, they can be engineered into components such as filters, couplers, impedance matchers, waveguides, resonators, and even spectrometers, capable of analyzing material properties through their interactions with light [4].

As operating frequencies increase, maintaining signal integrity becomes more challenging. Higher-frequency signals are characterized by shorter rise and fall times, which unfortunately exacerbate a phenomenon known as the skin effect. At low frequencies, current flows uniformly across the entire cross-section of a conductor. However, at higher frequencies, the current is pushed towards the surface, confining itself to a thin layer determined by the skin depth. This crowding of current creates a bottleneck effect, raising the conductor's resistance while simultaneously lowering its internal inductance. As a result, signals become distorted as they propagate through the interconnects [3].

Every network interconnection between electronic circuits introduces additional capacitive loads, leading to a degradation in circuit switching speeds. To accurately assess these parasitic effects, simulations must be conducted before any physical implementation. This requires the development of models that can translate real-world structures into equivalent electrical circuits, allowing for the evaluation of various effects caused by interconnections [5].

Analyzing high-speed connections within a chip demands a more advanced approach than traditional circuit analysis. Unlike circuits with lumped components, these interconnects behave like miniature transmission lines, where electrical properties depend on the signal frequency. Their behavior is best captured by an equivalent circuit model that includes distributed resistance (R), inductance (L), conductance (G), and capacitance (C) [6]. At high frequencies, the skin effect causes alternating current to concentrate near the surface of conductors, making conventional resistance calculations insufficient for predicting current opposition. To address this, we introduce the concept of 'skin impedance,' which accounts for the skin effect and provides a more accurate representation of resistance at high frequencies [3].

$$Z(x,s)=R+K\sqrt{s}$$

Researchers frequently replicate this phenomenon in both the spatial and time domains using the traditional Finite-Difference Time-Domain (FDTD) method in order to investigate it that is first introduced by Kane S. Lee [7]. However, the Courant-Friedrichs-Lewy (CFL) stability constraint, which results from the equally spaced separation of the voltage and current responses in both domains, limits the stability of the FDTD method. In particular, the spatial step size (Δx) directly determines the highest permissible time step (Δt_{max}),

and surpassing this CFL time limit makes the traditional FDTD approach unstable [6] [8]. To circumvent this constraint, we present the 'δ-method,' an unconditionally stable approach based on the FDTD framework that guarantees stability independent of time step size and bypasses the CFL constraint.

2 Proposed model formulation:

To model an interconnect while accounting for the skin effect at high frequencies, we employ the telegrapher's equations:

$$\frac{\partial V(x,t)}{\partial x}+RI(x,t)+L\frac{\partial I(x,t)}{\partial t}=0 \quad (1a)$$

$$\frac{\partial I(x,t)}{\partial x}+GV(x,t)+C\frac{\partial V(x,t)}{\partial t}=0 \quad (1b)$$

By applying the Laplace transformation to equations (1a) and (1b), we obtain:

$$\frac{\partial V(x,s)}{\partial x}+RI(x,s)+sLI(x,s)=0 \quad (2a)$$

$$\frac{\partial I(x,s)}{\partial x}+GV(x,s)+sCV(x,s)=0 \quad (2b)$$

Incorporating the skin effect into the equations, equation (2a) is modified as follows:

$$\frac{\partial V(x,s)}{\partial x}+Z_{int}(s).I(x,s)+sLI(x,s)=0 \quad (3)$$

Where $Z(s)=\alpha+\beta\sqrt{s}$, represents the impedance that accounts for the skin effect (skin impedance). After performing the inverse Laplace transformation, we obtain:

$$\frac{\partial V(x,t)}{\partial x}+Z_{int}(t)*I(x,t)+L\frac{\partial I(x,t)}{\partial t}=0 \quad (4a)$$

$$\frac{\partial I(x,t)}{\partial x}+GV(x,t)+C\frac{\partial V(x,t)}{\partial t}=0 \quad (4b)$$

The term $Z_{int}(t)*I(x,t)$ is expressed as:

$$Z_{int}(t)*I(x,t)=L^{-1}\left(Z_{int}(s).I(x,s)\right) \quad (5)$$

By substituting the expression for $Z_{int}(s)$ into equation (5):

$$Z(x,t)*I(x,t)=L^{-1}\left(\alpha.I(x,s)+\beta.I(x,s)\sqrt{s}\right) \quad (6a)$$

$$Z(x,t)*I(x,t)=L^{-1}\left(\alpha.I(x,s)\right)+L^{-1}\left(\beta.I(x,s)\sqrt{s}\right) \quad (6b)$$

$$Z(x,t)*I(x,t)=\alpha.I(x,t)+L^{-1}\left(\beta\frac{1}{\sqrt{s}}\right)*\frac{\partial I(x,t)}{\partial t} \quad (6c)$$

Note that $\sqrt{s}=\frac{s}{\sqrt{s}}$ and $L^{-1}\left(s.I(x,s)\right)=\frac{\partial I(x,t)}{\partial t}$.

$$L^{-1}\left(\beta\frac{1}{\sqrt{s}}\right)*\frac{\partial I(x,t)}{\partial t}=\beta\frac{1}{\sqrt{\pi t}}*\frac{\partial I(x,t)}{\partial t} \quad (6d)$$

$$L^{-1}\left(\beta\frac{1}{\sqrt{s}}\right)*\frac{\partial I(x,t)}{\partial t}=\beta\frac{1}{\sqrt{\pi}}\int_0^t\frac{1}{\sqrt{\tau}}\frac{\partial I(x,t-\tau)}{\partial(t-\tau)}d\tau \quad (6e)$$

If we assume that $\frac{\partial I(x,t-\tau)}{\partial(t-\tau)}=k(x,t-\tau)$, then we obtain:

$$\int_0^t\frac{1}{\sqrt{\tau}}\frac{\partial I(x,t-\tau)}{\partial(t-\tau)}d\tau=\int_0^t\frac{k(x,t-\tau)}{\sqrt{\tau}}d\tau=\int_0^{(n+1)\Delta t}\frac{k\left(x,(q+1)(\Delta t-\tau)\right)}{\sqrt{\tau}}$$

$$=\sum_{p=0}^{n}\int_{p\Delta t}^{(p+1)\Delta t}\frac{k\left(x,(q+1)(\Delta t-\tau)\right)}{\sqrt{\tau}}d\tau \quad (7)$$

Given that $k\left(x,(q+1)(t-\tau)\right)$ is constant, we get:

$$\sum_{p=0}^{q}\int_{p\Delta t}^{(p+1)\Delta t}\frac{k\left(x,(q+1)(\Delta t-\tau)\right)}{\sqrt{\tau}}d\tau$$

$$=\sqrt{\Delta t}\sum_{p=0}^{n}k\left(x,(q+1)(\Delta t-\tau)\right)\gamma_0(p) \quad (8)$$

Thus:

$$Z(x,t)*I(x,t)=\alpha.I(x,t)+\beta\frac{\sqrt{\Delta t}}{\sqrt{\pi}}\sum_{p=0}^{n}k\left(z,(q+1)(\Delta t-\tau)\right)\gamma_0(p) \quad (9)$$

Substituting equation (9) in (4a), we get:

$$\frac{\partial V(x,t)}{\partial x}+\alpha.I(x,t)+\beta\frac{\sqrt{\Delta t}}{\sqrt{\pi}}\sum_{p=0}^{n}k\left(z,(q+1)(\Delta t-\tau)\right)\gamma_0(p)$$

$$+L\frac{\partial I(x,t)}{\partial t}=0 \quad (10)$$

2.1 At any point in the middle of interconnects

To apply our proposed method, we first perform a spatial approximation of equations (4b) and (10). This results in the following approximations represented by equations (11) and (12), respectively:

$$\theta\left(v_{k+1}^{n+1}-v_k^{n+1}\right)+(1-\theta)\left(v_{k+1}^{n}v_k^{n}\right)+\frac{\alpha}{2}\Delta x\left(i_k^{n+1}+i_k^{n}\right)+$$

$$L\Delta x\frac{\partial i_k}{\partial t}+\beta\frac{\sqrt{\Delta t}}{\sqrt{\pi}}\sum_{p=0}^{n}k\left(z,(q+1)(\Delta t-\tau)\right)\gamma_0(p)=0 \quad (11)$$

$$\theta\left(i_k^{n+1}-i_{k-1}^{n+1}\right)+(1-\theta)\left(i_k^{n}-i_{k-1}^{n}\right)+\frac{G}{2}\Delta x\left(v_k^{n+1}+v_k^{n}\right)$$

$$+C\Delta x\frac{\partial v_k}{\partial t}=0 \quad (12)$$

2.2 Boundary conditions

For the boundary conditions, given that we apply the same boundary conditions at both ends, we derive the equations for the near-end and far-end boundaries from [9]:

The near-end equation:

$$i_1+\left(G\frac{\Delta x}{2}+G_s\right)v_1+\left(C\frac{\Delta x}{2}+C_s\right)\frac{\partial v_1}{\partial t}-G_sV_s=\frac{\Delta x}{2}I_s(x,t) \quad (13)$$

The far-end equation:

$$-i_{Nx}+\left(G_L+G\frac{\Delta x}{2}\right)v_{Nx+1}+\left(C_L+C\frac{\Delta x}{2}\right)\frac{\partial v_{Nx+1}}{\partial t}=\frac{\Delta x}{2}I_s(x,t) \quad (14)$$

2.3 Matrix form

We now combine equations (11), (12), (13), and (14) into a matrix equation, resulting in:

$$P_1I^{n+1}+P_2I^{n}+G^*\left(V^{n+1}+V^{n}\right)+C^*\frac{\partial V}{\partial t}+G_s^*V_S^*=0 \quad (15)$$

Here P_1, P_2, G^*, C^*, and G_s^* represent the matrices:

$$P_1=\begin{pmatrix}1/2 & 0 & \cdots & 0\\ -\theta & \theta & & \\ & \ddots & \ddots & \\ & & -\theta & \theta\\ & & & -1/2\end{pmatrix}_{m.(Nx+1)\times m.Nx}$$

$$P_2=\begin{pmatrix}1/2 & 0 & \cdots & 0\\ -(1-\theta) & 1-\theta & & \\ & \ddots & \ddots & \\ & & -(1-\theta) & 1-\theta\\ & & & -1/2\end{pmatrix}_{m.(Nx+1)\times m.Nx}$$

$$G^*=\frac{1}{2}\begin{pmatrix}G\frac{\Delta x}{2}+G_s & & & \\ & G\Delta x & & \\ & & \ddots & \\ & & & G_L+G\frac{\Delta x}{2}\end{pmatrix}_{m.(Nx+1)\times m.(Nx+1)}$$

$$C^*=\begin{pmatrix} C\frac{\Delta x}{2}+C_s & & & \\ & C\frac{\Delta x}{2} & & \\ & & \ddots & \\ & & & C_L+C\frac{\Delta x}{2} \end{pmatrix}_{m.(Nx+1)\times m.(Nx+1)}$$

$$G_s^*=\begin{pmatrix} -G_s & 0 & \cdots & 0 \\ 0 & 0 & & 0 \\ & & \ddots & 0 \\ 0 & & 0 & 0 \end{pmatrix}_{m.(Nx+1)\times m.(Nx+1)}$$

Here V^n and I^n denote the vectors:

$$V^n=\begin{bmatrix} v_1^n \\ v_2^n \\ \vdots \\ v_k^n \\ \vdots \\ v_{Nx+1}^n \end{bmatrix}_{m.(Nx+1)\times 1} \qquad I^n=\begin{bmatrix} i_1^n \\ i_2^n \\ \vdots \\ i_k^n \\ \vdots \\ i_{Nx}^n \end{bmatrix}_{m.Nx\times 1}$$

The matrix equation form of equation (11) is expressed as:

$$Q_1V^{n+1}+Q_2V^n+\alpha^*\left(I^{n+1}+I^n\right)+ L^*\frac{\partial I}{\partial t}+A\sum_{p=0}^{n}\frac{\partial I}{\partial(t-\tau)}\gamma_0(p)=0 \qquad (16)$$

Where Q_1, Q_2, α^*, L^*, and A are defined as follows:

$$Q_1=\begin{pmatrix} -\theta & \theta & & & \\ & -\theta & \theta & & \\ & & \ddots & \ddots & \\ & & & -\theta & \theta \end{pmatrix}_{m.Nx\times m.Nx}$$

$$Q_2=\begin{pmatrix} -(1-\theta) & 1-\theta & & & \\ & -(1-\theta) & 1-\theta & & \\ & & \ddots & \ddots & \\ & & & -(1-\theta) & 1-\theta \end{pmatrix}_{m.Nx\times m.Nx}$$

$$\alpha^*=\begin{pmatrix} \alpha\frac{\Delta x}{2} & & & \\ & \alpha\frac{\Delta x}{2} & & \\ & & \ddots & \\ & & & \alpha\frac{\Delta x}{2} \end{pmatrix}_{m.Nx\times m.Nx}$$

$$L^*=\begin{pmatrix} L\Delta x & & & \\ & L\Delta x & & \\ & & \ddots & \\ & & & L\Delta x \end{pmatrix}_{m.Nx\times m.Nx}$$

$$A=\begin{pmatrix} \beta\frac{\sqrt{\Delta t}\,\Delta x}{\sqrt{\pi}} & & & \\ & \beta\frac{\sqrt{\Delta t}\,\Delta x}{\sqrt{\pi}} & & \\ & & \ddots & \\ & & & \beta\frac{\sqrt{\Delta t}\,\Delta x}{\sqrt{\pi}} \end{pmatrix}_{m.Nx\times m.Nx}$$

2.4 Time approximation

We perform a time approximation of equations (15) and (16) and solve them to derive the following results:

$$V^{n+1}=N_1^{-1}\left\{N_2V^n-N_3I^n-G_s^*V_s^*+N_4\sum_{p=1}^{n}\gamma_0(p)\left\{I^{n+1-p}-I^{n-p}\right\}\right\} \qquad (19)$$

$$I^{n+1}=K_1^{-1}\left\{K_2I^n-Q_1V^{n+1}-Q_2V^n-\frac{A}{\Delta t}\sum_{p=1}^{n}\gamma_0(p)\left\{I^{n+1-p}-I^{n-p}\right\}\right\} \qquad (20)$$

Here, K_1, K_2, K_3, K_4 are defined as follows:

$$K_1=\left(\alpha^*+\frac{L^*}{\Delta t}+\frac{A}{\Delta t}\gamma_0(0)\right) \qquad K_2=\left(-\alpha^*+\frac{L^*}{\Delta t}+\frac{A}{\Delta t}\gamma_0(0)\right)$$

$$K_3=\left(G^*+\frac{C^*}{\Delta t}\right) \qquad K_4=\left(-G^*+\frac{C^*}{\Delta t}\right)$$

And N_1, N_2, N_3, N_4 are defined as follows:

$$N_1=K_3-P_1K_1^{-1}Q_1 \qquad N_2=K_4+P_1K_1^{-1}Q_2$$

$$N_3=P_2+P_1K_1^{-1}K_2 \qquad N_4=P_1K_1^{-1}\frac{A}{\Delta t}$$

3 Results And Discussion

This section investigates how well the proposed approach models three coupled interconnects, particularly in situations where the skin effect is substantial. We compare the method with the conventional FDTD technique to assess its performance. We begin by examining three identical interconnects with uniform coupling and losses. The electrical properties of these interconnects, described by per-unit-length parameter matrices, are sourced from existing literature [10]. This framework allows us to assess the accuracy and computational efficiency of the proposed method relative to the conventional FDTD approach.

$$\alpha=R_{dc}=\frac{1}{\sigma(tw)}I_{m*m}, \qquad \beta=\begin{pmatrix} \frac{1}{w+t} & 0 & 0 \\ 0 & \frac{1}{w+2t} & 0 \\ 0 & 0 & \frac{1}{w+t} \end{pmatrix}\sqrt{\frac{\mu}{\sigma}}$$

$$L=\begin{pmatrix} 1.6775 & 1.422 & 1.283 \\ 1.422 & 1.6775 & 1.422 \\ 1.283 & 1.422 & 1.6775 \end{pmatrix}\mu H/m$$

$$C=\begin{pmatrix} 121.57 & -78.78 & 0 \\ -78.78 & 200.35 & -78.78 \\ 0 & -78.78 & 121.57 \end{pmatrix}pF/m$$

$$G=0\ S/m$$

The geometry of the three-coupled interconnects is illustrated in Figure 1. The boundary elements are defined as follows:

$$R_s=\begin{pmatrix} 50 & 0 & 0 \\ 0 & 50 & 0 \\ 0 & 0 & 50 \end{pmatrix}\Omega \qquad R_L=\begin{pmatrix} 10 & 0 & 0 \\ 0 & 10 & 0 \\ 0 & 0 & 10 \end{pmatrix}K\Omega$$

$$C_s=\begin{pmatrix} 1 & 0 & 0 \\ 0 & 1 & 0 \\ 0 & 0 & 1 \end{pmatrix}fF \qquad C_L=\begin{pmatrix} 10 & 0 & 0 \\ 0 & 10 & 0 \\ 0 & 0 & 10 \end{pmatrix}fF$$

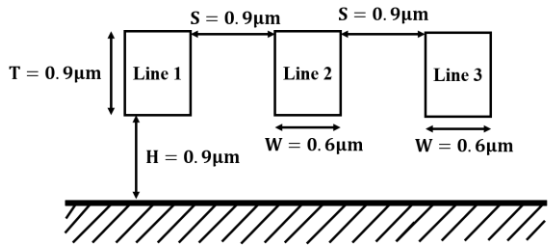

Fig. 1. Geometry of the three-coupled interconnects

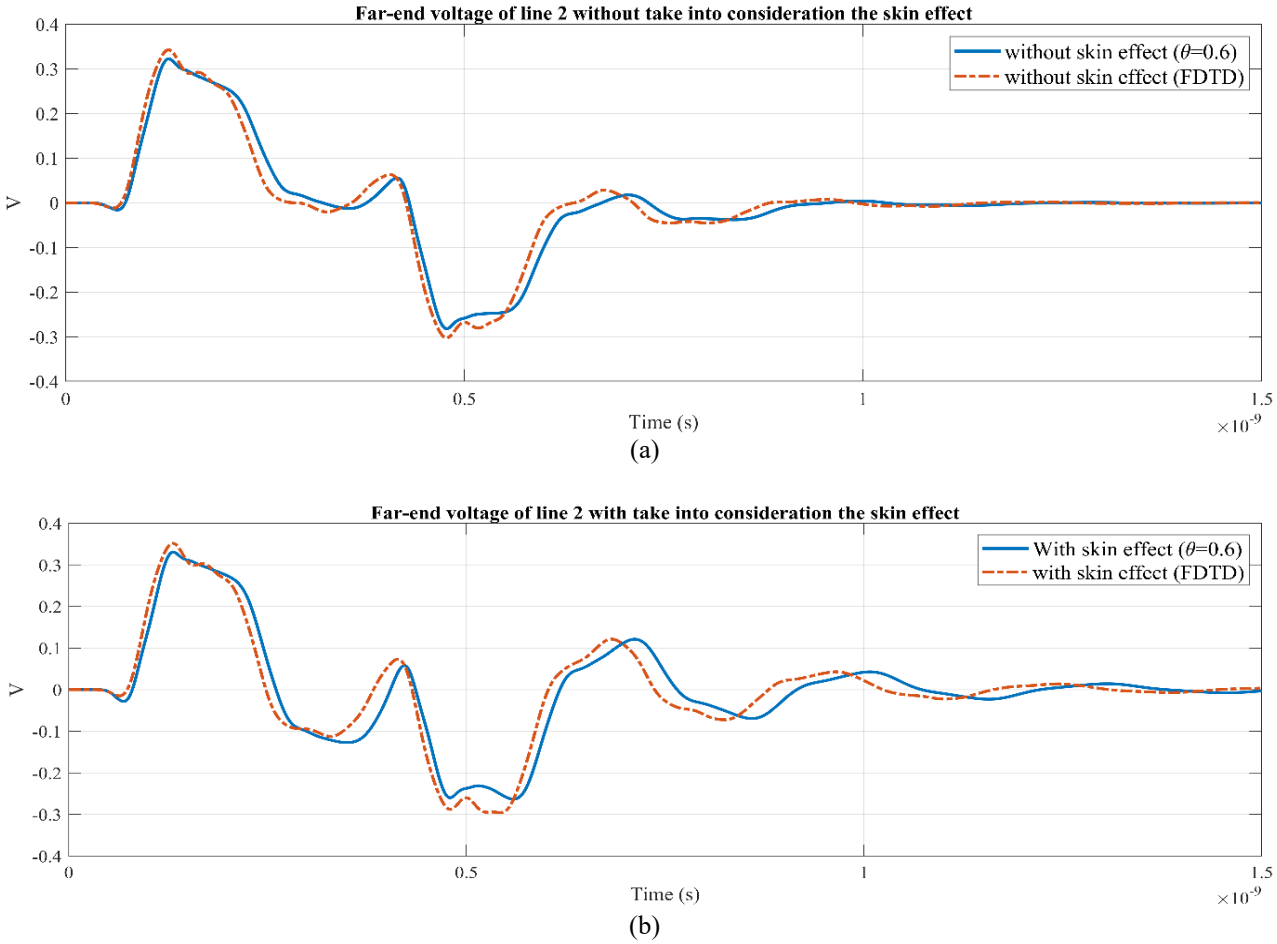

Fig. 2. Far-end voltage for line 2 (a) with skin effect and (b) without skin effect.

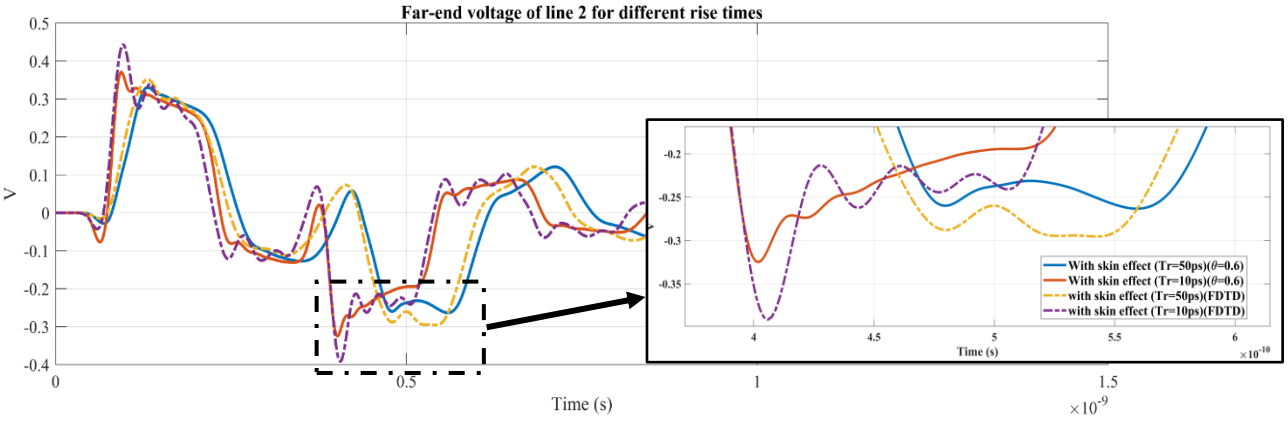

Fig. 3. Far-end voltage for line 2 for different rise time

V_{s1} is the input signal source applied to the first interconnect, characterized by a trapezoidal waveform with a rise time T_r=50 ps. Figure 2 displays the signal output of line 2, both with and without accounting for the skin effect.

In this section, we compare the results obtained using our proposed method (θ-method) with those from the conventional FDTD approach. Figures 2a and 2b show that our proposed method exhibits a high degree of similarity to the conventional FDTD in both scenarios: with and without accounting for the skin effect. This indicates that the proposed method offers comparable accuracy to the conventional FDTD.

To further assess the performance of our proposed method, we compare it with the conventional FDTD for different rise times, specifically T_r=50 ps and T_r=10 ps. These variations correspond to different frequencies, given that the maximum frequency is $f_{max}=\frac{1}{\pi T_r}$. This comparison is illustrated in Figure 3.

Similar to the previous figure, this one indicates that our proposed method exhibits a high degree of similarity to the conventional FDTD across different frequencies (corresponding to varying rise times T_r). However, it is also observed that our method shows less fluctuation in the peak values compared to the conventional FDTD, demonstrating improved accuracy, particularly at higher

frequencies (smaller T_r). To highlight the advantages of our proposed method, Table 1 presents a comparison of the simulation times between the conventional FDTD and our method. This comparison was conducted on a computer equipped with an Intel® Core™ i5-8365U CPU @ 1.60 GHz and 16 GB of RAM.

Table 1. Comparison of simulation time.

Simulation time (s)				
θ-method				**Conv-FDTD**
θ=0.5	**θ=0.6**	**θ=0.8**	**θ=1**	
3.48	3.62	3.65	3.70	50.93

From Table 1, it is evident that the proposed method demonstrates significantly shorter simulation times compared to the conventional FDTD. Specifically, our method achieves simulation times of 3.48 seconds for θ=0.5 and 3.65 seconds for θ=0.8, whereas the conventional FDTD takes 50.93 seconds. Moreover, the proposed method not only reduces simulation time but also offers enhanced accuracy and stability, making it a more efficient and reliable choice for time-domain simulations.

4 Conclusion

In conclusion, the proposed θ-method offers substantial improvements over the conventional FDTD approach in terms of simulation efficiency and accuracy. Our method significantly reduces computation time while maintaining or even enhancing accuracy, particularly at high frequencies where conventional methods often struggle. The comparative analysis demonstrates that the θ-method is a stable and reliable alternative, capable of effectively managing the complexities of interconnect modeling and outperforming traditional techniques in both speed and precision. This advancement highlights the method's potential for more efficient and accurate simulations in high-speed electronic circuit design.

References

1. J. Sunil, T. Shubham, C. Rajeevan, V. Munish, High Speed RLC Equivalent RC Delay Model Using Normalized Asymptotic Function for Global VLSI Interconnects. Microelectronics Journal. **107**, (2021)
2. R. Yenikepalli, R. K. Vobulapuram, Effect of Skin Impedance on Delay and Crosstalk in Lossy and Non-uniform On-Chip Interconnects. Intelligent Communication Control and Devices. 569-576, (2018)
3. N. J. K. Tulasi, V. Sulochana, K. V. Ramesh, R. K. Srinivasa, Modeling of CMS-based nonuniform interconnects using FDTD technique. Wiley. **47**, 11, 43-54, (2019)
4. V. Sulochana, A. Sunil, S. Balwinder, Performance Analysis of Lossy Coupled Non-uniform On-Chip Interconnects with Skin Effects. Circuits Systems and Signal Processing. **38**, 1413-1431, (2018)
5. K. Ait Belaid, H. Belahrach, A. Ghammaz, H. Ayad, Numerical analysis of lossy nonuniform interconnect lines in modern integrated circuits by multistep θ-method and Runge-midpoint method. Journal of Computational Electronics. **23**, 142-152. (2023)
6. C. Venkataiah; K. Satyaprasad; T. Jayachandra Prasad, Signal integrity analysis for coupled SWCNT interconnects using stable recursive algorithm. Microelectronics Journal. **74**, 13-23, (2018)
7. K. Yee, Numerical solution of initial boundary value problems involving Maxwell's equations in isotropic media, IEEE Transactions on Antennas and Propagation. **14**, 3, 302-307, (1966)
8. D. Gurijala, T. Madhavi, Crosstalk analysis of dielectric inserted side contact multilayer graphene nanoribbon interconnects for ternary logic system using unconditionally stable FDTD model. Microelectronics Journal. **133**, (2023)
9. M. Ait Errais, K. Ait Belaid, H. Belahrach, A. Zeroual, Numerical Analysis of Crosstalk Effects of Uniform Interconnect Lines Using theta-method. The International Conference on Global Aeronautical Engineering and Satellite Technology, Marrakesh, Morocco, April 24-26 (2024)
10. R. K. Vobulapuram, K. K. Brajesh, P. Amalendu, An accurate model for dynamic crosstalk analysis of CMOS gate driven on-chip interconnects using FDTD method. Microelectronics Journal. **45**, 14, 441-448, (2014)